Review Article

Ganjar Fadillah, Septian Perwira Yudha, Suresh Sagadevan, Is Fatimah*, Oki Muraza

Magnetic iron oxide/clay nanocomposites for adsorption and catalytic oxidation in water treatment applications

https://doi.org/10.1515/chem-2020-0159
received June 07, 2020; accepted July 17, 2020

Abstract: Physical and chemical methods have been developed for water and wastewater treatments. Adsorption is an attractive method due to its simplicity and low cost, and it has been widely employed in industrial treatment. In advanced schemes, chemical oxidation and photocatalytic oxidation have been recognized as effective methods for wastewater-containing organic compounds. The use of magnetic iron oxide in these methods has received much attention. Magnetic iron oxide nanocomposite adsorbents have been recognized as favorable materials due to their stability, high adsorption capacities, and recoverability, compared to conventional sorbents. Magnetic iron oxide nanocomposites have also been reported to be effective in photocatalytic and chemical oxidation processes. The current review has presented recent developments in techniques using magnetic iron oxide nanocomposites for water treatment applications. The review highlights the synthesis method and compares modifications for adsorbent, photocatalytic oxidation, and chemical oxidation processes. Future prospects for the use of nanocomposites have been presented.

Keywords: iron oxide, magnetic, nanomaterials, photocatalyst

1 Introduction

Water treatment has continued to be a required technology in many industries, because water contamination and pollution have become major environmental problems worldwide. This has created a great demand for an effective water treatment technology, and adsorption and photocatalysis are the most popular techniques due to their ease of handling. They are also more economical than other techniques. Research work in nanoscale science and engineering has suggested that nanomaterials have a great potential to improve the capability of these techniques to reduce water contaminants. Magnetic materials, especially iron oxide nanoparticles, have been known since ancient times to have characteristic properties for specified applications, including for water treatment [1]. Magnetite and maghemite (Fe_3O_4, γ-Fe_2O_3) are the most commonly studied materials due to the outstanding properties they exhibit on a nanometric scale, including high specific surface area, superparamagnetism, and so on [2–4]. The nanoscale dimensions of the materials can be developed by enhancing and functionalizing their surfaces for use in environmental and biomedical applications. In addition, magnetic nanocomposites have been developed for sensor, adsorption, catalytic, and photocatalytic environmental applications.

Magnetic iron oxide nanoparticles (MNPs) may be good candidates for use in the development of high-capacity adsorbents and photocatalysts. With their saturation magnetization, magnetic iron oxide-based nanocomposites provide a cost-effective approach for adsorption and photocatalysis through their reusability

* **Corresponding author: Is Fatimah,** Department of Chemistry, Faculty of Mathematics and Natural Sciences, Universitas Islam Indonesia, Kampus Terpadu UII, Jl. Kaliurang Km 14, Sleman, Yogyakarta, Indonesia, e-mail: isfatimah@uii.ac.id
Ganjar Fadillah: Department of Chemistry, Faculty of Mathematics and Natural Sciences, Universitas Islam Indonesia, Kampus Terpadu UII, Jl. Kaliurang Km 14, Sleman, Yogyakarta, Indonesia
Septian Perwira Yudha: Department of Chemistry, Materials for Energy and Environment Research Group, Universitas Islam Indonesia, Kampus Terpadu UII, Jl. Kaliurang Km 14, Sleman, Yogyakarta, Indonesia
Suresh Sagadevan: Nanotechnology & Catalysis Research Centre, Deputy Vice Chancellor (Research & Innovation), University Malaya, Malaysia
Oki Muraza: Center of Research Excellence in Nanotechnology and Chemical Engineering Department, King Fahd University of Petroleum & Minerals, Dhahran, 31261, Saudi Arabia

and ease of recovery. A material's selectivity or affinity for a specified contaminant can be enhanced by modifying its surface and combining it with features of solid supports. By the scheme, and as conducted in biomedical and biological applications of MNPs, material properties can be tailored by setting synthesis parameters [4,5].

Some solid supports have been reported as magnetic nanoparticle supports, such as zeolite, MCM-41, biochar, carbon nanotube, and mesoporous silica. Among potential supports and materials that can be combined with magnetic properties and MNPs, clay and clay minerals have received interest. Clays have a high adsorption capacity, which corresponds to the high surface area resulting from their layer structure and a net negative charge on their structure, which attracts and holds cations, such as heavy metals and cationic molecules. There are three basic classes of clay, which are as follows: kaolinite, micas (for example, illite), and smectites (for example, montmorillonite) [6,7]. Clays, especially natural clays, are attractive and low-cost materials due to their porosity, high specific surface area, and capacity to adsorb organic molecules and ions. At the time of writing, increasing attention on the use of magnetic iron oxide/clay nanocomposites (MICNCs) was evident in the SCOPUS database (Figure 1).

The physicochemical properties of MICNCs depend on their source, the kind of clay they contain, and the parameters governing their synthesis [8–11]. The layer silicate structure, cation exchange capacity, and pore size distribution of nanocomposites affect critical features for specified purposes in water treatment. To understand variability in nanocomposite formation and the implications for the use of nanocomposites as engineered materials, this review has presented an overview of our present knowledge regarding the influence of source material, synthesis method, and parameters in production technologies on MICNCs.

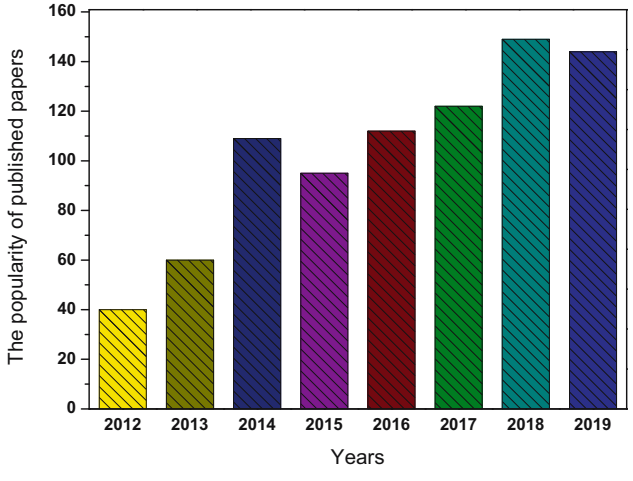

Figure 1: The popularity of using MICNCs for the photodegradation of organic molecules (keywords: magnetic iron oxide/clays; source: www.scopus.com, 2012–2019).

2 Synthesis of MICNCs

Clay minerals have been defined as hydrated phyllosilicates, which are abundant in sedimentary rocks. The basic unit of phyllosilicates, including clay minerals, is based on interconnected SiO_4^{4-} tetrahedrons, with three apical oxygen atoms from each tetrahedron shared with another tetrahedron, making the fourth apical oxygen vertically positioned upon the sheet [12,13]. In this respect, the basic structure is $Si_2O_5^{2-}$ with hexagonal symmetry. In some clays, the tetrahedral position can be occupied by aluminum atoms, which deform the tetrahedral sheet and decrease its symmetry to a level lower than hexagonal.

The tetrahedron forms sheets with X $(O, OH)_6$ octahedrons, which share not only vertexes but also half of their edges. Octahedrons are tagged together by the octahedron plane perpendicularly to [001], so that three anions (O^- or OH^-) form a lower layer, and three anions are in the upper layer and in between the octahedral cations (X). The occupation of structural positions in the octahedral sheet generates trioctahedral sheet silicates in which each O or OH is surrounded by three divalent cations, like Fe(II) or Mg(II), and dioctahedral sheet silicates in which each O or OH ion is surrounded by two trivalent cations, mostly Al(III). Clay can be divided into two major classes according to the combination of tetrahedral and octahedral sheets, type 1:1 (layers t-o) and type 2:1 (layers t-o-t).

Many combinations and substitutions of the layers affect the negative charges of the main structure. Clay minerals are classified according to the following criteria: (i) type of layer (1:1 or 2:1), (ii) type of interlayer (water or interlayer cation), (iii) layer charge, (iv) type of octahedral sheet (di- or trioctahedral), and (v) chemical composition. In an analogous structure, layered double hydroxides (LDHs) have been designated as "anionic clay" and have a general formula expressed as $[M^{2+}_{1-x}M^{3+}_x(OH)_2]^{x+}A_{x/n}{}^{n-}\cdot mH_2O$, where M^{2+} and M^{3+} represent, respectively, di- and trivalent metal cations; A^{n-} represents a charge anion n; x represents the molar ratio between di- and trivalent cations $M^{2+}/(M^{2+} + M^{3+})$; and m represents the number of water molecules. These criteria

Table 1: Clay minerals, specific procedures, and synthesis parameters of MICNCs

Clay mineral	MNP precursor	Method	Synthesis condition	Notes	Ref.
Natural bentonite from Slovakia	Not mentioned	Co-precipitation	Iron oxide is precipitated at 20°C and 85°C	Composites have a high specific surface area. The highest magnetization is 46.22 emu/g, present at a 1:1 ratio of bentonite to iron	[14]
Bentonite	$FeCl_3$ and $FeSO_4$	Co-precipitation	Iron oxide precipitation is followed by drying at 100°C for 3 h in air	Composites have good adsorption of Cd, Zn, Cu, and Ni	[15]
Montmorillonite from Greece	$FeCl_3{\cdot}6H_2O$	Co-precipitation and acetic acid treatment	Montmorillonite is mixed with $FeCl_3{\cdot}6H_2O$ and NaOH, followed by exposure to glacial acetic acid	Composites have a saturation magnetization of 4.1 emu/g and more basal spacing than montmorillonite d_{001}	[16]
Kaolin	Fe^{2+} and Fe^{3+}	Impregnation	Iron oxide nanoparticles are dispersed into a kaolin suspension in the presence of chitosan	Composites have a good adsorption capability for ciprofloxacin	[16]
Saponite and palygorskite	Fe_3O_4	Impregnation	Fe_3O_4 slurry is adsorbed by saponite and palygorskite, followed by drying at 60–80°C	Composites have a good ability to adsorb the surfactant from water	[17]
Natural bentonite from Slovakia	$FeSO_4{\cdot}7H_2O$ and $FeCl_3{\cdot}6H_2O$	Co-precipitation	Bentonite/iron oxide weight ratios of 1:1 and 5:1 with co-precipitation temperatures of 20°C and 85°C	Magnetic iron oxide/bentonite composites have a magnetization of about 35–42 emu/g, and iron oxide is formed as the γ-Fe_2O_3 phase	[14]
Natural bentonite from Shanghai	$FeSO_4$–HNO_3	Pillarization–co-precipitation	Montmorillonite is pillared with Al, prior to MNP co-precipitation		[18]
Natural bentonite from Ethiopia	$FeCl_3{\cdot}6H_2O$–$FeSO_4{\cdot}7H_2O$	Co-precipitation–oxidation	The $FeCl_3{\cdot}6H_2O$–$FeSO_4{\cdot}7H_2O$ precursor solution is co-precipitated into activated bentonite, followed by drying at 100°C		[19]
Fe_3O_4/activated montmorillonite	$FeCl_3{\cdot}6H_2O$ and $FeCl_2{\cdot}4H_2O$	Co-precipitation	A 30% ammonia solution is added dropwise to the iron solution ($n_{Fe^{2+}}$:$n_{Fe^{3+}}$ = 1:1.8) at 363 K with constant stirring to adjust the pH to 9–10, so that Fe^{2+}/Fe^{3+} ions are precipitated. Mt powder is then added, and the solution is stirred for 4 h	The material has significantly improved in the adsorptivity for MB	[20]
Diatomite	$FeCl_3{\cdot}6H_2O$	Solvothermal	The MNP precursor is prepared by mixing $FeCl_3{\cdot}6H_2O$ with ethylene glycol, followed by the addition of	Composites have a saturation magnetization of 26.89 emu/g	[21]

Table 1: Continued

Clay mineral	MNP precursor	Method	Synthesis condition	Notes	Ref.
			$CH_3COONa{\cdot}3H_2O$. The mixture is kept in an autoclave for 8 h at 200°C		
Illite	$FeCl_3{\cdot}6H_2O$	Solvothermal		Composites have a saturation magnetization of 35.39 emu/g	[21]
Natural bentonite from Slovakia	$FeSO_4{\cdot}7H_2O$ and $FeCl_3{\cdot}6H_2O$ (with the molar ratio of $Fe^{3+}/Fe^{2+} = 2$)		Co-precipitation is followed by drying at 70°C	Iron oxide is in the γ-Fe_2O_3 phase	[22]
Montmorillonite	$FeCl_3{\cdot}6H_2O$–$FeCl_2{\cdot}4H_2O$	Pillarization	The precursor of the oligomer of iron oxide is formed by mixing Fe(III) and Fe(II) solution with ammonia. Montmorillonite is intercalated by cetyltrimethylammonium ions in combination with tetraethyl orthosilicate	MNPs are homogeneously distributed and generally spherical in shape, and particle sizes are around 10–15 nm	[23]
Montmorillonite SWy-2	$FeCl_2{\cdot}4H_2O$	Pillarization–impregnation	Montmorillonite is pillared with Ti, followed by Fe impregnation	The specific saturation magnetization is influenced by the temperature of calcination	[24]
Natural bentonite from Argentina	$Fe(NO_3)_2$	Pillarization	The intercalation of oligomer ferrous hydroxide is followed by calcination at 500°C	Increasing basal spacing d_{001} of bentonite was obtained significantly	[25]
Montmorillonite K10	$FeCl_2{\cdot}4H_2O$	Pillarization	The intercalation of oligomer ferrous hydroxide is followed by calcination at 400°C for 2 h	Increasing basal spacing d_{001} of montmorillonite from 1.25 to 1.5 Å was identified	[26]
Natural bentonite from East Java, Indonesia	$FeCl_3$	Pillarization	The intercalation of oligomer ferrous hydroxide is followed by calcination at 400°C for 4 h	The process increased the basal spacing d_{001} of montmorillonite from 1.49 to 1.69 Å	[27]
K10 montmorillonite	$FeCl_2{\cdot}4H_2O$	Co-precipitation–hydrothermal	The precipitate is obtained by mixing montmorillonite suspension and $FeCl_2{\cdot}4H_2O$–NH_4OH and keeping the mixture in an autoclave at 140°C for 5 h	Dispersed spherical Fe_3O_4 nanoparticles in the 10–45 nm size range are coated on the surface of the montmorillonite	[28]
Montmorillonite	$FeSO_4{\cdot}7H_2O$–$FeCl_3$	Co-precipitation–hydrogel formation	After magnetic iron oxide montmorillonite is obtained, the graft copolymerization of acrylamide is performed using potassium persulfate as a free radical initiator and *N*,*N*′-methylenebisacrylamide as a cross-linking agent	The magnetic nanocomposite has hydrophilicity and the ability to swell	[29]

Table 1: Continued

Clay mineral	MNP precursor	Method	Synthesis condition	Notes	Ref.
Laponite	$FeSO_4{\cdot}7H_2O$–$FeCl_3$	Co-precipitation–hydrogel formation	Fe^{3+}:Fe^{2+} at a molar ratio of 2:1 is co-precipitated into a laponite suspension by the addition of NH_4OH at 70°C for 2 h. Hydrogel is formed via a cross-linking reaction using ammonium persulfate and *N*,*N*,*N*′,*N*′-tetramethylethylenediamine	The magnetic nanocomposite has hydrophilicity and the ability to swell	[30]
Sepiolite	$FeCl_2{\cdot}4H_2O$	Hydrothermal	The precursor of $FeCl_2{\cdot}4H_2O$ solution is heated in an autoclave at 140°C for 4 h in a mixture with NH_4OH and sepiolite suspension. Then, the precipitate is dried at 60°C for 24 h		[31]
Kaolin	$FeCl_3{\cdot}6H_2O$–$FeSO_4{\cdot}7H_2O$	Co-precipitation	The precursor of $FeCl_3{\cdot}6H_2O$–$FeSO_4{\cdot}7H_2O$ solution is stirred at 70°C for 2 h in a mixture with NaOH and a suspension of kaolin. The precipitate is dried at 115°C	Composites have well-distributed Fe_3O_4 nanoparticles, ranging in size from 5.76 to 18.2 nm with a good adsorption capability	[32]
Kaolinite	$FeSO_4{\cdot}7H_2O$	Co-precipitation–microwave irradiation	$FeSO_4{\cdot}7H_2O$ precursor solution is stirred in a mixture with NaOH and subjected to microwave irradiation (700 W, 2450 MHz) for 10 min. The formed Fe_xO_y NPs are mixed with a kaolinite suspension while stirring, and the mixture is dried completely at 40°C	Fe_xO_y phases–maghemite (γ-Fe_2O_3) in a mixture with magnetite (Fe_3O_4) phase are formed and anchored on the edges of the kaolinite	[33]
Kaolinite	$FeCl_3{\cdot}6H_2O$ and $FeSO_4{\cdot}7H_2O$	Co-precipitation	$FeCl_3{\cdot}6H_2O$: $FeSO_4{\cdot}7H_2O$ in a molar ratio of 2:1 is mixed with NH_4OH and slowly added to kaolinite. The mixture is stirred for 5 h, followed by drying at 70°C for 24 h		[34]
Haloysite	$FeCl_3{\cdot}6H_2O$ and $FeSO_4{\cdot}7H_2O$	Co-precipitation	A suspension of HNT is mixed with $FeCl_3{\cdot}6H_2O$–$FeSO_4{\cdot}7H_2O$, followed by the dropwise addition of NH_3H_2O solution at 60°C in N_2	HNT–Fe_3O_4 has good magnetic properties with a saturation magnetization of 27.91 emu/g at a magnetic field of about 9,000 Oe	[35]
Pristine HNT	$Fe(NO_3)_3{\cdot}9H_2O$	Wet impregnation	A pristine HNT suspension is stirred with $Fe(NO_3)_3{\cdot}9H_2O$, followed by the rapid removal of the solvent at 80°C		[36]

Table 1: Continued

Clay mineral	MNP precursor	Method	Synthesis condition	Notes	Ref.
Magnetic and anionic–cationic modified montmorillonite (Fe_3O_4–cetyltrimethylammonium chloride–sodium eicosenoate/CTMAC/SEIA-Mt)	$FeCl_3$–$FeCl_2$	Co-precipitation–surfactant modification	The preparation is calcined for 1 h at 200°C under high-purity argon flow Montmorillonite is intercalated using CTMA and SEIA, prior to co-precipitation using $FeCl_3$–$FeCl_2$ precursor solution	The material has a great adsorption capacity for the removal of the MB dye and a saturation magnetization of 19.84 emu/g	[37]

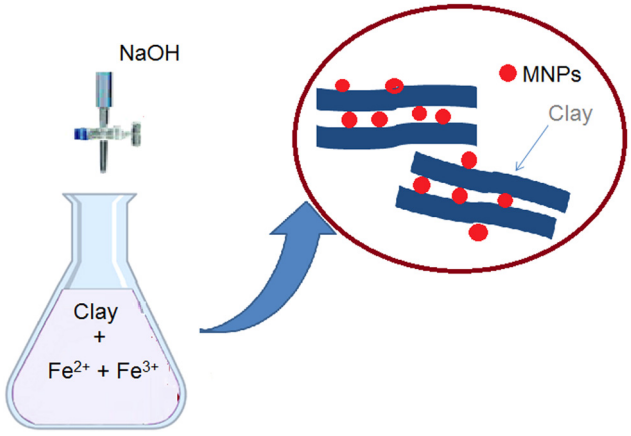

Figure 2: Schematic representation of the co-precipitation method.

affect the synthesis procedure and variables. Table 1 shows the clay minerals, specific procedures, and synthesis parameters of various MICNCs. In general, there are two main synthesis procedures, co-precipitation and the intercalation of MNPs into a clay structure.

The co-precipitation method is based on the chemical reaction used to produce magnetic nanoparticles in aqueous clay mineral dispersions, so the nucleation and growth of nanoparticles occur in situ in an aqueous dispersion of clay minerals, as described in Figure 2. The synthesis of nanocomposites by co-precipitation involves mixing clay mineral with MNP precursors under alkaline condition to form a sol–gel system. NH_4OH and/or NaOH are commonly used to create the alkaline condition, which directly produces the precipitate of the composite [14,33,34]. The interaction between MNPs produced from clay minerals in a sol–gel system can be intensified using several methods, such as heating in a reflux system or microwave-irradiation. As the precipitate is created, drying or calcination can be conducted, which influences the iron oxide phase and magnetization properties through various processes. Synthesis using Slovakian bentonite has shown that a higher drying temperature (85°) successfully produces the γ-Fe_2O_3 phase with a magnetization of 35–42 emu/g, while at a lower temperature (20°C), iron oxide presents in the oxo-hydroxide phase (goethite) and has a low magnetization (8–15 emu/g). The combination of co-precipitation and oxidation can also be conducted to find a homogeneous MNP phase [18,38]. Instead of using iron salt as a precursor, an aqueous oxidation using $NaNO_3$ as an oxidant has been used to form Fe_3O_4 nanoparticles (Fe_3O_4 NPs). The homogeneous phase of iron oxide can be obtained by conducting precipitation and oxidation under N_2 flow and the use of ultrasound-irradiation for the intensification.

Pillarization is another method of nanocomposite formation (Figure 3). In pillarization, MNPs are formed through the intercalation of polyoxocations or iron oxide oligomer precursors on to the interlayer structure of smectite clay, followed by calcination. For example, Tirelli reported the use of the oligomer trinuclear acetate–hydroxo iron(III) nitrate, which was obtained through the slow titration of Fe(II) in alkaline conditions as an MNP precursor [39]. As with the pillarization of other metal oxides, the intercalation of the oligomer into a clay suspension was conducted by stirring vigorously. Mixing iron salt with urea also creates oligomers [26]. The success of clay pillarization can be identified by determining the basal spacing d_{001}, using the basal spacing d_{001} of smectite clay as a reference.

The pillarization of smectite is advantageous, because it increases its basal spacing and pore distribution, bringing it from micro- to macroporosity. To facilitate the formation of MNPs in the clay structure, montmorillonite that has been pillared with another metal oxide, such as aluminum, silica, or titanium oxide, can be used [23,24,40]. Increasing the specific surface area and pore volume through pillarization using aluminum oxide facilitates the distribution of MNPs, which enhances the adsorption mechanism in contribution for the Photo-Fenton oxidation process of the dye. Measuring saturation magnetization has shown that decreasing the loading of Fe_3O_4 NPs decreases particle size and saturation magnetization. This trend is analogous with the relationship between the saturation magnetization and coercivity (H_c) of Fe_3O_4 NPs. A higher Fe_3O_4 nanoparticle size reflects a higher saturation magnetization and H_c. The low magnetization of materials with a smaller particle size is due to the formation of a magnetically disordered surface as a result of the large surface-to-volume ratio. However, the saturation magnetization values of these composites are still acceptable (23.5–81.2 emu/g), though they are less than those of Fe_3O_4 nanoparticles (82.7 emu/g). The magnetization, a higher specific surface area, and a resultant lower particle size of the composite for RhB decolorization enhance its adsorption capability and photocatalytic activity [18]. The composite's iron loading, magnetization, and temperature of calcination significantly affect the size of MNPs [24,40]. In addition, the use of titanium-pillared montmorillonite as a support for MNPs has shown that increasing the temperature of calcination increases particle size and saturation magnetization [24].

Kaolinite is a 1:1 clay structure that has a small capacity for cation exchange and does not swell. Its structure has rarely been reported to involve the intercalation of metal oxides or their precursors. This different structure means that MNPs/kaolinite materials are mainly prepared using the co-precipitation method, which is also used in the production of halloysite, pristine halloysite, and halloysite nanotubes (HNTs), which are within the kaolin–serpentine class of clay.

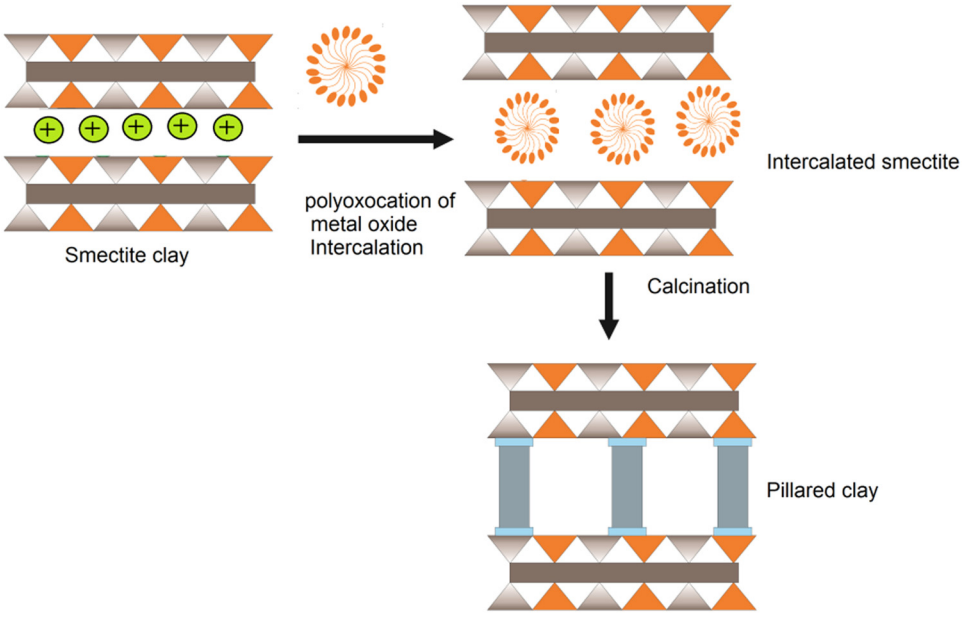

Figure 3: Schematic representation of clay pillarization.

MNPs in the composite could be formed via a similar synthesis route as bentonite, which is produced by mixing precursors with a kaolinite suspension or preparing them separately before their dispersion into the suspension. The combination of co-precipitation and hydrothermal processes for nanoparticle formation has also been reported to produce homogeneously distributed nanoparticles. Different mechanisms of MNP growth have been reported, from impregnation methods to the use of pristine HNTs [36].

The structure of pristine HNTs consists of gibbsite octahedral sheet groups (Al–OH) on the internal surface and siloxane groups (Si–O–Si) on the external surface. This structure results in a negatively charged outer surface and a positively charged inner lumen in solutions with a pH of less than 8.5. The impregnation method applies a charged iron oxide precursor at the outer surface of HNTs. As the precursor on the outer surface is exposed to acetic acid vapor, iron acetate precursor species are formed. Calcination converts these species into smaller sized nanoparticles. Figure 3 shows the nanoparticle formation on the HNT surface.

LDHs are characterized as a porous clay with the potential to form nanocomposites, and their layers and ionic structures have different characteristics. The crystalline structure of LDHs consists of positively charged layers $[M^{2+}_{1-x}M^{3+}_{x}(OH)_2]^{x+}$ similar to the layered structure of brucite ($Mg(OH)_2$) and an interlayered negative region composed of anions and water molecules, $A^{n-}_{x/n}{\cdot}mH_2O$. As a result of this different ionic condition, magnetic nanocomposite formation with LDH usually involves anionic surfactants in the intercalation step [41]. Though the formation of magnetic nanocomposites with hydrotalcite (HT) can be identified by the increasing basal spacing of the interlayered structure, they are mostly synthesized using the co-precipitation method. The formation of magnetic HT reported by Miranda (2014), Lulu (2014), and Zolfaghar (2012) are examples of this method, as are hydrothermal and solvothermal syntheses [41–44].

Through the co-precipitation method, MNPs are dispersed in the interlayer space of the clay structure, but scanning electron microscope and transmission electron microscope analyses have shown that they are mostly distributed on to the clay surface. Generally, the pH, the temperature, and the concentration of the alkali and iron oxide precursors are critical factors in the synthesis. These factors significantly affect the nucleation and growth of particles. For example, MNPs will have different sizes and surface properties when synthesized from different iron-to-clay mass ratios and at different temperatures of nucleation.

Surface modification has been used to influence MICNCs' ability to adapt to various pH conditions and hydrophobicities of the treated solution. The formation of hydrogels, hydrophobic magnetic nanocomposites, and surfactant-modified magnetic nanocomposites are three major techniques that have been widely reported. The hydrophobicity of MICNCs can be increased through the formation of Fe_3O_4–CTMAC/SEIA–Mt. In this process, prior to co-precipitation, montmorillonite is intercalated using cetyltrimethylammonium and sodium eicosenoate. The interlayer space was increased through the use of CTMA as a cationic surfactant. The electrostatic attraction of clay platelets may create an exfoliated composite system, meaning that the surfactant breaks the parallel arrangement. A multi-arrangement consists of monolayers, bilayers, and pseudo trilayers, and a paraffinic structure may be created. In addition, the use of CTMA as a cationic surfactant with SEIA as an anionic surfactant has been proposed as a way to stabilize the hydrophobic interaction of organic molecules at the surface [33].

The hydrogel formation of MICNCs from laponite and montmorillonite has been reportedly conducted by cross-linking the polymerization method [29,30]. As iron oxide/montmorillonite is produced, the hydrogel form is synthesized through the in situ graft copolymerization of acrylamide using potassium persulfate as a free radical initiator and *N*,*N*′-methylenebisacrylamide as a cross-linking agent. Polymerization agents were mixed with the nanocomposite suspension. Similarly, MNPs in laponite have been subjected to the cross-linking reaction through the use of ammonium persulfate as a radical initiator with *N*,*N*,*N*′,*N*′-tetramethylethylenediamine reagent to form poly(*N*-isopropylacrylamide) hydrogel. Hydrogels have a better solubility, pH stability, and mechanical and diffusion properties, which create a viscous, suspended treated solution with a highly concentrated contamination.

3 Application of MICNCs in water and wastewater treatments

In water treatment, MICNCs have been widely used for the removal of pollutants from aqueous solution, either by adsorption, photooxidation, or by chemical oxidation processes. The reduction and removal of contaminants, including chemical constituents, such as dye, heavy metals, and other organic pollutants from water, have been reported.

3.1 Adsorption

The use of MICNCs for the treatment of water and wastewater via adsorption is more dominant than photocatalysis and advanced oxidation processes (AOPs). The combination of the adsorptive properties of clay minerals with the magnetic properties of MNPs to produce novel MICNC adsorbents is a promising technique for the removal of pollutants from water. Table 2 shows various MICNCs along with their target contaminants and removal processes. The next section discusses each process in brief detail.

As seen in Table 2, many modifications have been attempted to enhance the adsorption capability of MICNCs, mainly through surface functionalization. The application of surfactants, polymers, and other compounds containing functional groups on to nanocomposites is effective for attracting the adsorbate. To describe the adsorption behavior, studies have adopted isotherm models, including the Langmuir, Freundlich, and Dubinin–Radushkevich models. As seen in Table 2, the Langmuir isotherm model is the most representative for almost all kinds of adsorbates. The Langmuir isotherm model represents the monolayer adsorption occurring on an energetically uniform surface, on which adsorbed molecules are not interactive. The equilibrium is attained once the monolayer is completely saturated. Contrary to Langmuir, the Freundlich model describes adsorption on an energetically heterogeneous surface, on which adsorbed molecules are interactive. In a different approach, the Dubinin–Radushkevich (D–R) model was constructed, based on the assumption that the adsorption performance is preferable when it occurs in micropores by pore-filling rather than layer-by-layer surface coverage. The D–R model can generally be applied to adsorption that occurs via a van der Waals interaction, for example, the adsorption of Hg(II) by Fe_3O_4/Al-pillared bentonite [44]. Three main mechanisms for the adsorption of organic compounds have been identified, which are as follows:

a. π–π interactions are those that are available for surface-modified MICNCs, especially by the surfactant. In addition, hydrogen bond formation between MICNCs and double bonds of the adsorbate are usually both present together [37,62]. In a study on the adsorption of oxytetracycline by MABC, adsorption kinetics and Fourier-transform infrared spectroscopy revealed the π–π interaction mechanism. The enthalpy of adsorption at 12.50 kJ/mol represents the physical adsorption interaction dominantly. Moreover, positive values of ΔS° revealed an increasing randomness at the solid–solution interface during the adsorption process. Similarly, the hydrophobic interaction in phenol (PHE), CRE, and *p*-cresol (PCS) adsorption was presumably from the hydrogen bonds between the dodecyl sulfate/β-cyclodextrin (DS/β-CD) cavity contained in Fe/HT–dodecyl sulfate/β-cyclodextrin (DS/β-CD)Fe/HT–DS/β-CD and the phenolic compounds forming inclusion complexes, which promote selective adsorption.
b. Hydrogen bonding corresponds to the interaction between the hydrogen of the hydroxyl group (–C(O)–OH) in dyes or organic compounds and the oxygen atoms in the tetrahedral layer of the montmorillonite surface. Hydrogen bonding dominates when there is an adsorbate electrophilic element in the functional group, such as the nitrogen in, for example, $-N(C_2H_5)_2$ or the oxygen atom.
c. Lewis interaction occurs when the nitrogen atom in the dye or organic molecule, which acts as the Lewis base, combines with the Al^{3+} and Fe^{3+} ions on the MICNC surface, which act as the Lewis acid. This molecular dynamic of this interaction is simulated by Ouachtak for the adsorption of rhodamine B and has also been found in the adsorption of picloram herbicide by pillared montmorillonite [73].

A schematic representation of the possible interaction between adsorbate and MICNCs is presented in Figure 5.

In previous research work, FTIR analysis has revealed that the interaction between iron oxide and pillared montmorillonite occurs through the nitrogen of the pyridine ring as a result of the replacement of OH groups from the coordination sphere of iron. As shown in Figure 6, the interaction involves the formation of a bridge complex between COO^- ions, nitrogen atoms in pyridine groups, and iron(III) centers, such as those previously proposed [72].

3.2 Photocatalytic and catalytic degradation of organic pollutants

MNPs are capable of oxidizing in AOPs. Traditional AOPs based on hydroxyl radicals (•OH) and sulfate radicals ($SO_4^{\bullet-}$) produce strong oxidation radicals for the degradation of organic pollutants in water [74]. Electron excitation in MNPs activates the formation of radicals when MNPs are exposed to a small amount of energy, such as when undergoing thermal treatment. MICNCs are common catalyst carriers with high specific surface areas

Table 2: MICNCs used for adsorption

MICNCs	Contaminant	Saturation magnetization/M_s (emu/g)	Isotherm of adsorption	Removal capacity	Ref.
Fe_3O_4/ZnAl–LDH	Cr(VI)	Not presented	Langmuir	197.1	[45]
MNPs/bentonite	La^{3+}, Eu^{3+}, and Yb^3	14.0°	Langmuir	18.4 mg/g for La(III), 26.1 mg/g for Eu(III), and 71.4 mg/g for Yb(III)	[46]
Fe_3O_4/montmorillonite	Methylene blue (MB)	Not presented	Langmuir	59.9	[20]
Graphene/magnetite/montmorillonite	MB	63.48	Langmuir	225.0	[47]
Fe_3O_4/Al-pillared bentonite	Hg(II)	22.08	Dubinin–Radushkevich (D–R)	26.2 mg g^{-1}	[48]
Fe_3O_4 NPs/diatomite and Fe_3O_4 NPs/illite	PO_4^{3-}	35.39	Langmuir	11.9 mg/g for Fe_3O_4 NPs/diatomite and 5.48 mg/g for Fe_3O_4 NPs/illite	[21]
Fe_3O_4/bentonite	Enrofloxacin	27.57	Not presented	180.0 mg/g	[49]
Chitosan/clay/magnetite	Cu(II) and As(V)	Adsorption		Cu(II) and As(V) of 17.2 and 5.9 mg g^{-1} in the initial concentration ranges of 16–656.0 and 17–336.0 mg L^{-1}, respectively	[38]
Fe_2O_3–palygorskite	Fenarimol	Adsorption		27.8 mg/g	[50]
Fe_3O_4–sepiolite	Bisphenol A	Photo-Fenton		Maximum removal of 12.0 mg/g at room temperature	[51]
Di(2-thylhexly)phosphoric acid–immobilized magnetic GMZ bentonite	Eu(III)	Adsorption		40.5 mg/g	[52]
Fe_3O_4/HNT	Methylene blue (MB), neutral red (NR), and methyl orange (MO)			37.3, 30.6, and 2.5 mg/g for MB, NR, and MO, respectively	[35]
Sodium dodecyl sulfate-modified BiOBr/magnetic bentonite	Tetracycline and ciprofloxacin	Photocatalysis		18.5 mg/g for TC and 34 mg/g for CP	[53]
REC–Fe_3O_4	MB and NR	Adsorption		8.6 mg MB, 16.0 mg NR	[54]
Fe_3O_4/sepiolite	Atrazine	31.82	Langmuir	15.9	[55]
Fe_3O_4/HNT	Cr(VI)	29.53	Not presented	38.6	[56]
Fe_3O_4/bentonite	Cr(III)	Not presented	Langmuir	11.7	[57]
Fe_3O_4/saponite	Malachite green, Congo red, and indigo carmine,	Not presented	Langmuir	159.1 mg/g for MG, 73.1 mg/g for CR, and 110.3 mg/g for IC	[58]
Magnetic bentonite/carboxymethyl chitosan/sodium alginate hydrogel beads	Cu(II)	18.86 emu/g	Langmuir	56.8 mg/g	[59]
$MnFe_2O_4$/bentonite	Acid red	Not presented	Not presented	23.5 mg/g	[60]
Fe_3O_4/kaolinite	Copper, lead, cadmium, chromium, and nickel	38.2	Langmuir	Cu^{2+} = 106.0 mg/g Pb^{2+} = 98.0 mg/g Cd^{2+} = 100.0 mg/g Cr^{2+} = 97.0 mg/g Ni^{2+} = 95.2 mg/g	[61]

Table 2: Continued

MICNCs	Contaminant	Saturation magnetization/M_s (emu/g)	Isotherm of adsorption	Removal capacity	Ref.
Magnetic attapulgite–biochar composite (MABC)	Oxytetracycline	31.46	Langmuir	33.3 mg/g	[62]
Fe_3O_4/bentonite	Cd(II)	Not presented	Langmuir	63.3 mg/g	[14]
Iron oxide–HT modified with the surfactant dodecyl sulfate (DS) and β-cyclodextrin (β-CD)	PHE, *p*-nitrophenol (PNP), and PCS	Not presented	Langmuir	PHE = 216.1 mg/g PNP = 255.6 mg/g PCS = 272.5 mg/g	[63]
γ-Fe_2O_3/halloysite	Ag nanoparticles	18	Langmuir	67.9 mg/g	[64]
Magnetic and anionic–cationic modified montmorillonite (Fe_3O_4–CTMAC/SEIA–Mt)	Methylene blue	19.84	Langmuir	211 mg/g	[37]
Fe_3O_4/halloysite	Naphthol green B	Not presented	Langmuir	11.2 mg/g	[65]
Polyethylenimine functionalized magnetic montmorillonite clay (MMT–Fe_3O_4–PEI)	Cr(VI)	59.81	Langmuir	62.9 mg/g	[28]
Fe_3O_4/sepiolite	Safranin	31.8	Langmuir	18.5 mg/g	[66]
Magnetic core-shell dodecyl sulfate intercalated layered double hydroxide (Fe_3O_4@DS-LDH)	MB and MO	25	Freundlich	MB = 225.0 mg/g MO = 221.0 mg/g	[67]
CTAB-modified Fe_3O_4/montmorillonite	2,6-Dichlorophenol and *p*-nitrophenol	5.4	Langmuir	200 mg/g for 2,6-dichlorophenol and 125.0 mg/g for *p*-nitrophenol	[67]
Fe_3O_4/montmorillonite	MB	Not presented	Langmuir	223.0 mg/g	[25]
Montmorillonite–Cu(II)/Fe(III) oxides	Humic acid	3.9	Langmuir	98.0 mg/g	[68]
Clay/polyaniline/Fe_3O_4	MB	36.52	Langmuir	184.0 mg/g	[69]
O,*O*′-bis(2-aminopropyl) polypropyleneglycol-γ-Fe_2O_3/ montmorillonite	MO	26.7		9.8 mg/g	[70]
Fe_3O_4/bentonite	Co(II)	Not presented	Langmuir	10.7 mg/g	[71]
Fe_2O_3/bentonite	Picloram	Not presented	Langmuir		[72]

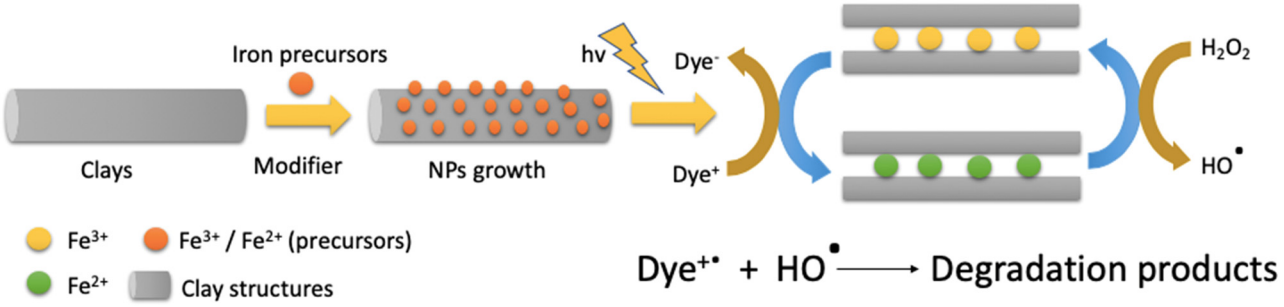

Figure 4: Schematic representation of the possible mechanism in adsorption using MICNCs.

and good thermal stability and ion-exchange performance. They support the adsorption mechanism via oxidation over a heterogeneous catalyst. Zong et al. (2020) used magnetic clay with persulfate to degrade atrazine. In their study, Fe_3O_4 was loaded on sepiolite clay to catalyze potassium persulfate ($K_2S_2O_8$) and hydrogen peroxide (H_2O_2), generating $SO_4^{\cdot 2-}$ and $^{\cdot}OH$ for atrazine removal [75]. The composite maintained a good catalytic activity and stability during four consecutive runs. The quenching experiments showed that $SO_4^{\cdot 2-}$/$^{\cdot}OH$ and $^{\cdot}OH$ were the dominant radical species in the two systems.

The photocatalytic activity of MNPs arises from the semiconductor properties of Fe_2O_3 and Fe_3O_4. As semiconducting materials, both oxides are promising visible light-driven photocatalysts due to the band gap energy range. Moreover, iron oxides have a low cost and an excellent chemical stability, besides being easy to produce and environment-friendly. They also absorb most visible light. For example, γ-Fe_2O_3 absorbs light up to 600 nm, collects up to 40% of solar spectrum energy, and is one of the cheapest semiconductor materials. However, the stability of iron oxide photocatalysts is more or less at a pH of more than 3, and depending on the chemical environment, iron oxides may easily lose activity due to corrosion and aggregation.

Drawbacks of using these oxides in photocatalysis arise from the recombination of separated photo-induced electron–hole pairs due to a low band gap energy. The formation of oxides in nanosize, in

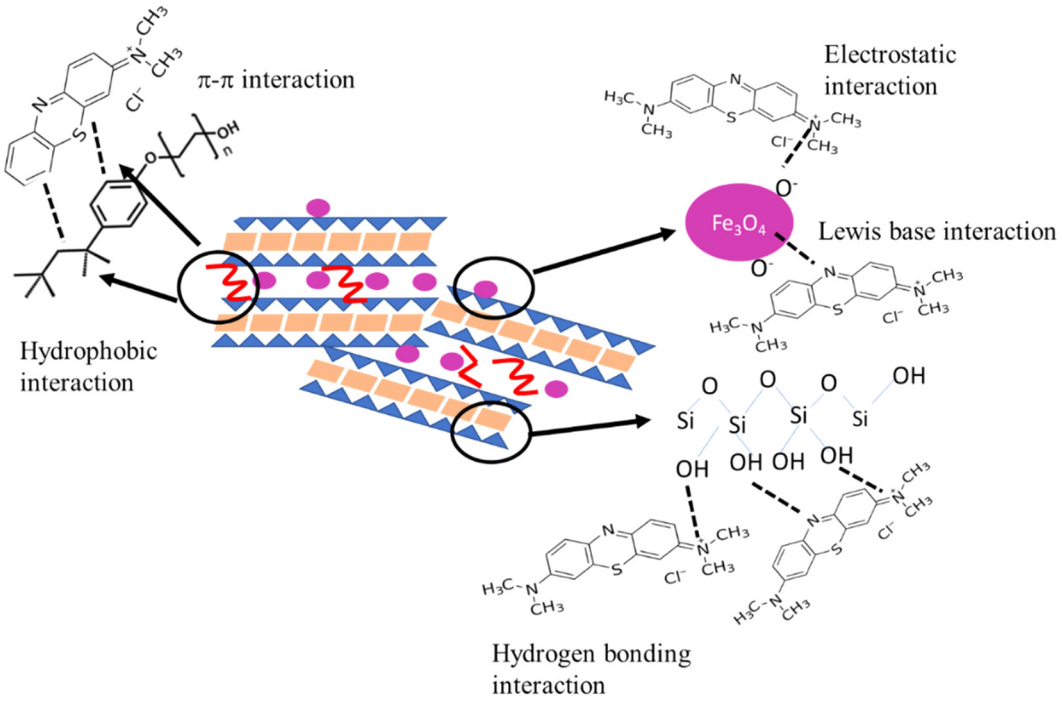

Figure 5: Montmorillonite (Mt.)-supported iron shifts base complexes as a catalyst.

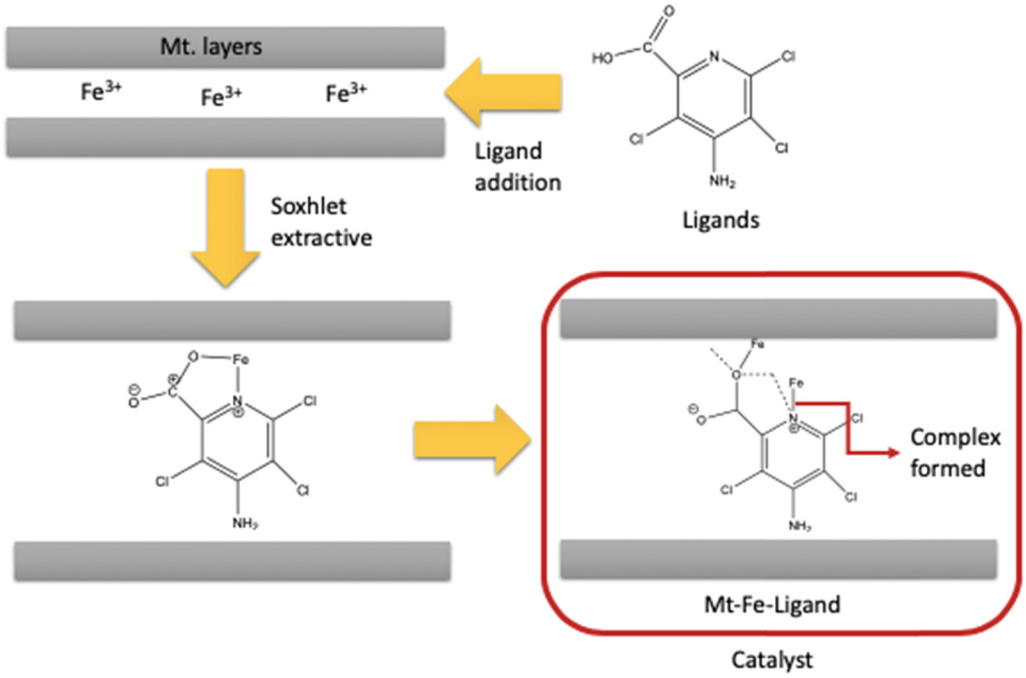

Figure 6: Schematic representation of the photocatalysis mechanism over MNPs.

combination with the supporting form, has proven effective in improving the separation efficiency of photo-induced electron–hole pairs. According to the method given in Figure 7, as MNP and MICNC photocatalysts are exposed by photons, electrons are excited from the valence band (VB) to the conductance band (CB), leading to the formation of a hole (h^+) in the VB. The interaction between h^+ and e^- in each CB and VB with OH and O_2 from the reaction system or solvent produces radicals for further oxidation.

Wang et al. (2017) reported that the formation of Fe_2O_3–Fe_3O_4 nanocomposites supported by montmorillonite increased the band gap energy [83]. Fe_2O_3–Fe_3O_4/Mt has a band gap energy of 2.85 eV, while pure Fe_2O_3–Fe_3O_4 has a band gap energy of 2.14 eV. Increasing the band gap energy increases the photocatalytic degradation of Fe_2O_3–Fe_3O_4/Mt by methyl orange which is higher compared to the pure one. The composite shows a 1.61-fold degradation rate, compared to pure Fe_2O_3–Fe_3O_4, and 98.8% recoverability by magnetic separation. Figure 4 shows a schematic representation of the photocatalytic degradation of organic molecules by MNP and MICNC photocatalysts.

Bledowski et al. reported that the redox potential of the CB of Fe_2O_3 is around 0.2 eV and that because the band gap energy of MICNCs is 2.85 eV, the VB is located at 3.15 eV. The CB has a lower redox potential than the formation of superoxide anion radicals ($O_2^{\bullet-}$) [$E^0(O_2/O_2^{\bullet-})$ = −0.33 eV. The spontaneous formation of $O_2^{\bullet-}$ and $HOO^{\bullet-}$ arises, because O_2 interacts with excited electrons. Moreover, the interaction of the electron hole with H_2O to produce $HO^{\bullet}$ occurs, because the VB has a higher potential reduction than the oxidation of water [E^0 ($H_2O/^{\bullet}OH$) = 2.38 V] [86]. These generated radicals are effective oxidants for the degradation of dyes and organic compounds. A further oxidation reaction releases CO_2, H_2O, NO^{3-}, and SO^{3-} upon completion. In addition, fast degradation can be achieved through the addition of an oxidant, mainly H_2O_2. Interactions between H_2O_2 and the surface of MICNCs are mainly initiated by the following chain of reactions:

$$H_2O_2 + \equiv Fe(II) \rightarrow \equiv Fe^{3+}OH + OH^-$$
$$\equiv Fe^{3+} + H_2O_2 \rightarrow \equiv Fe^{3+}(H_2O_2)$$
$$\equiv Fe^{3+}(H_2O_2) \rightarrow (\equiv Fe^{2+} \cdot O_2H)$$
$$(\equiv Fe^{2+} \cdot O_2H) \rightarrow \equiv Fe^{2+} + HO_2^{\bullet}/HO_2^{\bullet-}$$

In addition, $^{\bullet}OH$, $HO_2^{\bullet}/HO_2^{\bullet-}$ ions are generated through the reactions, which are responsible for the reversible conversion between Fe^{2+} and Fe^{3+}. Furthermore, modifications on to iron oxide/clay have been reported concerning the catalyst and photocatalyst stabilization and surface modification to improve hydrophobicity.

Electronic features of dispersed Fe have been studied by Bao et al. [76], who showed that the amount and location of iron oxide nanoparticles in MICNCs are critical parameters in determining the shape, size, and crystal structure of nanoparticles, which correlate with

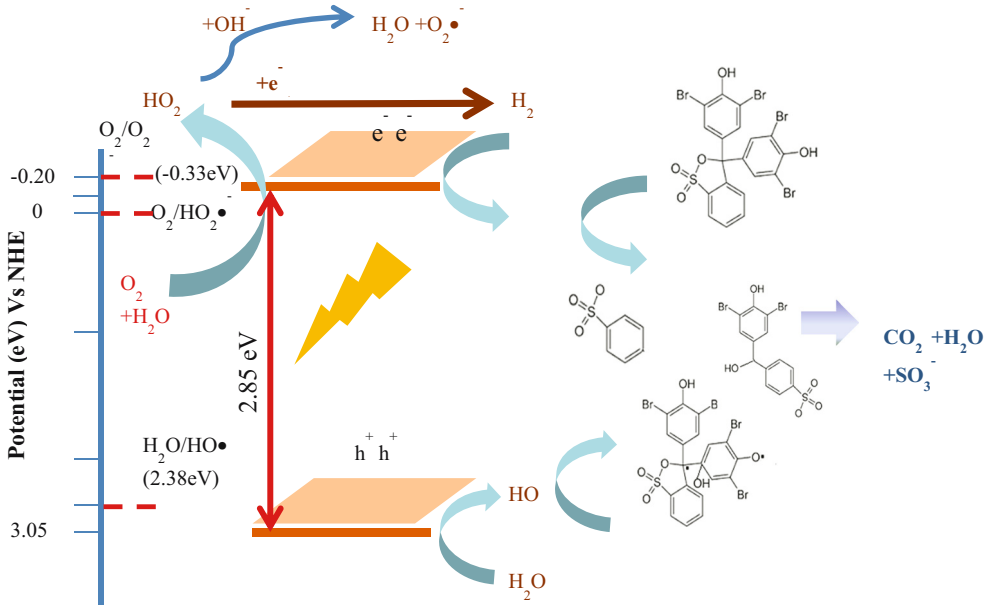

Figure 7: Mechanism of the photocatalytic degradation of organic molecules using iron oxide/clay nanocomposites.

their magnetization. It was concluded that the zero valence and large surface area of iron oxide nanoparticles create a high level of photocatalytic activity. The larger specific surface area facilitates an intensive interaction in the oxidation mechanism, and the calcination process creates a particle size uniformity and a strong interaction of iron oxide with the clay support. The strengthened interaction of iron oxide with a silica–alumina framework in the clay support reduces iron leaching, giving it a stable activity for consecutive usage as shown by the Fenton-like phenol degradation. Increasing calcination temperature increases particle size, and at certain temperatures, it affects iron oxide agglomeration and phase change [84].

Visible light sensitization is a popular and efficient photocatalysis mechanism that saves energy. The materials doping with Ag, Co, and TiO_2 in small portions significantly enhance photocatalytic activity through the inhibition of electron recombination [78,82]. As photocatalysts have good capability in the visible light region, this photocatalytic process could be sunlight-driven.

4 Physicochemical character of MICNCs

Specific surface area and pore distribution are important parameters in adsorbent and photocatalyst applications for water treatment [60]. The higher specific surface area provides more adsorption sites for interacting with target molecules. The Brunauer–Emmett–Teller approach calculated from the N_2 adsorption/desorption isotherm data is a generally acceptable method for this calculation. However, specific surface area and pore size distribution are not the most influential parameters for removal efficiency, as surface hydrophobicity and hydrophilicity also play roles in the interaction [27].

In practice, several factors influence intensive adsorption, such as pH, adsorbent/catalyst dosage, time of treatment, and so on. For example, pH determines the efficiency of surface–adsorbate bonding, which is an important step in adsorption, and it depends on the zeta potential of the adsorbent surface. The zeta potential is correlated with saturation magnetization. Measurements of zeta potential in solutions under the influence of magnetic fields have shown that increasing the field greatly influences the adsorption of dyes and metals, with larger field strengths creating more adsorption [25,49]. Magnetic fields exert much influence on the adsorption of dyes, as shown by their increase of removal and adsorption capacity. In addition, increasing nanoparticle size increases saturation magnetization [87]. Nanoparticle size analysis can be carried out using transmission electron microscopy (Table 3).

Szabo concluded that the lamellar sizes and cation exchange capacities of clay minerals affect MNP growth and magnetization. Comparing the formation of MNPs in laponite with their formation in montmorillonite showed

Table 3: MICNCs for the photocatalytic degradation of organic compounds

Material	M_s	Process	Target compound	Degradation efficiency (%)	MNP size	Ref.
Sepiolite/Fe_3O_4	Not given	AOP using $K_2S_2O_8$	Atrazine	57.8		[75]
Fe_3O_4/rectorite	30.28	Wet peroxidation	*p*-Chlorophenol	98		[76]
Magnetite/HNTs	Not given	AOP using $NaIO_4$	Pentachlorophenol	89	15–30	[36]
Fe_3O_4/montmorillonite	27.57	AOP using $K_2S_2O_8$	Enrofloxacin	90	30–150	[49]
Fe_3O_4/montmorillonite	78	AOP using permonosulfate	Bisphenol A (BPA)	99.3	45–58	[77]
TiO_2/montmorillonite/Fe_3O_4	23.96	Photocatalysis	MB	94	45–60	[78]
Fe_3O_4/montmorillonite	Not given	Photocatalysis	Brilliant orange X-GN	79.1 (under visible light exposure)	Not given	[78]
Fe/montmorillonite	41 emu/g	Photocatalysis	RhB	79	<10	[79]
Fe_3O_4/palygorskite	44.11	Photocatalysis	Tetracycline	72.9	20–50	[80]
Sepiolite/Fe_3O_4	Not given	Photocatalysis	Diuron	92	5–20	[81]
Sepiolite/Fe_3O_4	Not given	Photocatalysis	BPA	87	2–50	[51]
Polypyrrole/HNTs/Fe_3O_4/Ag/Co nanocomposite	Not given	Photocatalysis	MB	91	10–20	[82]
Fe_2O_3–Fe_3O_4/montmorillonite	Not given	Photocatalysis	Methyl orange	98.8	10–80	[83]
Maghemite/montmorillonite	45.61	Photocatalysis	Phenol	99	25–30	[84]

that the size effect and greater amount of aggregation in laponite composites were related to the dominance of the maghemite phase due to the greater contribution of attractive dipolar interactions between magnetic nanocrystals [87]. Compared to laponite, montmorillonite sheets accommodated the formation of nanoparticles, while in the laponite, formed particles had the tendency to produce highly exfoliated clay lamellae. Thus, MNPs in laponite have a higher saturation magnetization than MNPs in montmorillonite. Saturation magnetization data have shown that the following factors significantly influence the properties of MICNCs:

a. MNP content and phase.
b. Average particle size of MNPs, size distribution, and aggregation state.
c. Specific surface area and the porous structure of clay.
d. Homogeneous/heterogeneous dispersion of iron oxide crystals in the clay matrix.

Figure 8 shows the effect of the iron content in iron oxide on montmorillonite-based MICNCs with saturation magnetization recapitulated from several references. In general, the higher the iron content in MICNCs, the higher the saturation magnetization. Higher particle sizes and the formation of more aggregates tend to give a higher saturation magnetization, and a higher calcination temperature enhances saturation magnetization [24,79]. The MNP size depends on the amount of iron precursors and the growth of iron oxide crystallite. As the growth of nanoparticles occurs in the layers of the clay structure, layer charge, and porous and surface structure are crucial factors that suppress nanoparticle formation. Nanoparticle formation is also controlled by temperature, especially in the synthesis of iron oxide-pillared clay, as a phase change from γ-Fe_2O_3 to α-Fe_2O_3 may occur, which affects magnetization properties. α-Fe_2O_3 decreases magnetization, while the presence of zerovalent iron (Fe^0) in MICNCs increases magnetization [84,88].

Surface characteristics, including hydrophobicity, pore distribution, pore radius, and nanoparticle distribution, are critical parameters in the proposed MICNC interactions in

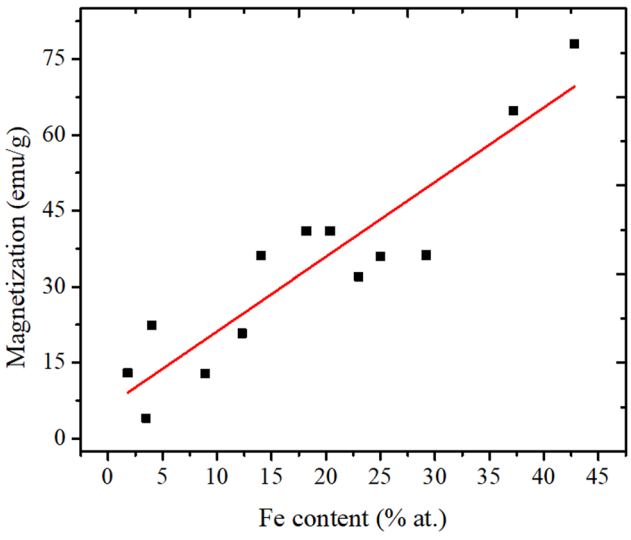

Figure 8: Effect of the iron content on saturation magnetization in montmorillonite-based MICNCs.

the adsorption mechanism. Theoretically, higher specific surface areas provide more space for adsorption. The data presented in Table 1 show that the insertion of MNPs into clay structure oxides changes the specific surface area of the composite. As with magnetization, iron content influences porous distribution and thus, the specific surface area of the composite. However, dispersion method, including pillarization, co-precipitation, and impregnation, is a more important factor than the iron content. The MNPs are distributed as metal oxide pillars in the pillarization method, while co-precipitation and impregnation position nanoparticles in the interlayer or at the edge of silica or alumina layers [27,88]. The cation exchange capacity and surface area of raw clay, as well as the layered structure, calcination temperature, and dispersion method, strongly influence the specific surface area of the composite. As there are so many additional factors, there is no strict relationship between magnetization and the specific surface area of MICNCs.

The terms recoverability and sustainability of the adsorbent and photocatalyst materials are proven by reusability. In most reported works, the durability of the materials until a minimum of five cycles with less reduction of removal activity has been presented. However, in photocatalytic applications, electronic transition may affect changes in the electronic state of MNPs in a nanocomposite. X-ray photoelectron spectroscopy is an effective method for predicting the change in speciation.

5 Future of MICNCs

MICNC syntheses and applications in water and wastewater treatments have been well studied and have been used in various ways to deal with pollutant-containing water. Research work has shown that incorporating functional MNPs into clay structures has resulted in stable adsorbent, catalyst, and photocatalyst materials, which have increased recoverability and sustainability in the treatment process. However, to our knowledge, research work has not addressed large-scale applications of this technology. Thus, we have recommended that researchers study large-scale production and implementation, including the following:

a. Research works should address the technical form of materials in large-scale processes. Although the adsorption capability of MICNCs has been discussed, findings have been limited to a laboratory setting. Modeling and simulation have shown that the performance of materials on a larger scale may vary from that on a smaller scale due to changes in material activity and the economic cost of the process.
b. Studies should recalculate the economic availability of technologies using MICNCs. The main factors for redesigning systems and technology in water and wastewater treatments are pH and the chemical and biological stability of the water treated.
c. Consideration should be given to potential secondary pollution and further treatment.

Conflict of interest: Authors declare no conflict of interest.

References

[1] Anderson NJ, Bolto BA, Dixon DR, Kolarik O, Priestley AJ, Raper WGC. Water and wastewater treatment with reusable magnetite nanoparticles. Water Sci Technol. 1982;14:1545–6.
[2] Abdullah NH, Shameli K, Abdullah EC, Abdullah LC. Low cost and efficient synthesis of magnetic iron oxide/activated sericite nanocomposites for rapid removal of methylene blue and crystal violet dyes. Mater Charact. 2020;163:110275. doi: 10.1016/j.matchar.2020.110275.
[3] Zhu N, Ji H, Yu P, Niu J, Farooq MU, Akram MW, et al. Surface modification of magnetic iron oxide nanoparticles. Nanomaterials. 2018;8:1–27. doi: 10.3390/nano8100810.
[4] Abdullah NH, Shameli K, Abdullah EC, Abdullah LC. Solid matrices for fabrication of magnetic iron oxide nanocomposites: synthesis, properties, and application for the adsorption of heavy metal ions and dyes. Compos Part B Eng. 2019;162:538–68. doi: 10.1016/j.compositesb.2018.12.075.
[5] Pereira MC, Oliveira LCA, Murad E. Iron oxide catalysts: fenton and fenton-like reactions – a review. Clays Clay Min. 2012;47:285–302.
[6] Herney-Ramírez J, Madeira LM. Use of pillared clay-based catalysts for wastewater treatment through fenton-like processes. In: Gil A, Korili SA, Trujillano R, Vicente MA. Pillared clays and related catalysts. New York: Springer; 2010. doi: 10.1007/978-1-4419-6670-4.
[7] Xu A, Yang M, Yao H, Du H, Sun C. Rectorite as catalyst for wet air oxidation of phenol. Appl Clay Sci. 2009;43:435–8. doi: 10.1016/j.clay.2008.10.003.
[8] Zhou CH. An overview on strategies towards clay-based designer catalysts for green and sustainable catalysis. Appl Clay Sci. 2011;53:87–96. doi: 10.1016/j.clay.2011.04.016.
[9] Abuzerr S, Darwish M, Mahvi AH. Simultaneous removal of cationic methylene blue and anionic reactive red 198 dyes using magnetic activated carbon nanoparticles: equilibrium, and kinetics analysis. Samer Abuzerr Maher Darwish
Amir Hossein Mahvi. 2017;534–45. doi: 10.2166/wst.2018.145.
[10] Hadjltaief HB, Da Costa P, Beaunier P, Gálvez ME, Zina MB. Fe-clay-plate as a heterogeneous catalyst in photo-Fenton

oxidation of phenol as probe molecule for water treatment. Appl Clay Sci. 2014;91–92:46–54. doi: 10.1016/j.clay.2014.01.020.
[11] Virkutyte J, Varma RS. Eco-friendly magnetic iron oxide-pillared montmorillonite for advanced catalytic degradation of dichlorophenol. ACS Sustainable Chem Eng. 2014;2:1545–50. doi: 10.1021/sc5002512.
[12] Sanchis R, Cecilia JA, Soriano MD, Vázquez MI, Dejoz A, Nieto JL, et al. Porous clays heterostructures as supports of iron oxide for environmental catalysis. Chem Eng J. 2018;334:1159–68. doi: 10.1016/j.cej.2017.11.060.
[13] Kalmakhanova MS, Diaz de Tuesta JL, Massalimova BK, Gomes HT, Kalmakhanova MS, de Tuesta JL, et al. Pillared clays from natural resources as catalysts for catalytic wet peroxide oxidation: characterization and kinetic insights. Environ Eng Res. 2019;25:186–96. doi: 10.4491/eer.2018.402.
[14] Orolínová Z, Mockovčiaková A. Structural study of bentonite/iron oxide composites. Mater Chem Phys. 2009;114:956–61. doi: 10.1016/j.matchemphys.2008.11.014.
[15] Oliveira LC, Rios RV, Fabris JD, Sapag K, Garg VK, Lago RM. Clay-iron oxide magnetic composites for the adsorption of contaminants in water. Appl Clay Sci. 2003;22:169–77. doi: 10.1016/S0169-1317(02)00156-4.
[16] Bourlinos AB, Karakassides MA, Simopoulos A, Petridis D. Synthesis and characterization of magnetically modified composites. Chem Mater. 2000;12:2640–5. doi: 10.1088/1742-6596/1091/1/012024.
[17] Makarchuk OV, Dontsova TA. Removal of anionic surfactants from wastewater by magnetic mineral sorbents. J Water Secur. 2016;2:1–9.
[18] Wan D, Li W, Wang G, Petridis D. Size-controllable synthesis of Fe_3O_4 nanoparticles through oxidation-precipitation method as heterogeneous fenton catalyst. J Mater Res. 2016;31:2608–16. doi: 10.1557/jmr.2016.285.
[19] Belachew N, Bekele G. Synergy of magnetite intercalated bentonite for enhanced adsorption of congo red dye. Silicon. 2020;12:603–12. doi: 10.1007/s12633-019-00152-2.
[20] Chang J, Ma J, Ma Q, Zhang D, Qiao N, Hu M, et al. Adsorption of methylene blue onto Fe_3O_4/activated montmorillonite nanocomposite. Appl Clay Sci. 2016;119:132–40. doi: 10.1016/j.clay.2015.06.038.
[21] Chen J, Yan LG, Yu HQ, Li S, Qin LL, Liu GQ, et al. Efficient removal of phosphate by facile prepared magnetic diatomite and illite clay from aqueous solution. Chem Eng J. 2016;287:162–72. doi: 10.1016/j.cej.2015.11.028.
[22] Danková Z, Fedorová E, Bekényiová A. Bentonite/iron oxide magnetic composites: characterization and application as Pb (II) adsorbents. Arch Tech Sci. 2017;1:65–75. doi: 10.7251/afts.2017.0916.065d.
[23] Çiftçi H, Ersoy B, Evcin A. Pillared magnetite/clay structures as a function of CTAB and TEOS concentration. Emerg Mater Res. 2020;9:1–7. doi: 10.1680/jemmr.18.00148.
[24] Bachir C, Lan Y, Mereacre V, Powell AK, Koch CB, Weidler PG. Magnetic titanium-pillared clays (Ti-M-PILC): Magnetic studies and mössbauer spectroscopy. Clays Clay Min. 2009;57:433–43. doi: 10.1346/CCMN.2009.0570404.
[25] Tireli AA, Marcos FCF, Oliveira LF, do Rosário Guimarães I, Guerreiro MC, Silva JP. Influence of magnetic field on the adsorption of organic compound by clays modified with iron. Appl Clay Sci. 2014;97–98:1–7. doi: 10.1016/j.clay.2014.05.014.
[26] Virkutyte J, Varma RS. Eco-friendly magnetic iron oxide-pillared montmorillonite for advanced catalytic degradation of dichlorophenol. ACS Sustainable Chem Eng. 2014;2:1545–50. doi: 10.1021/sc5002512.
[27] Fatimah I, Nurkholifah YY. Physicochemical and photocatalytic properties of Fe-pillared bentonite at various fe content. Bull Chem React Eng Catal. 2016;11; doi: 10.9767/bcrec.11.3.456.398-405.
[28] Fayazi M, Ghanbarian M. One-pot hydrothermal synthesis of polyethylenimine functionalized magnetic clay for efficient removal of noxious Cr(VI) from aqueous solutions. Silicon. 2020;12:125–34. doi: 10.1007/s12633-019-00105-9.
[29] Mahdavinia GR, Afzali A, Etemadi H, Hoseinzadeh H. Magnetic/pH-sensitive nanocomposite hydrogel based carboxymethyl cellulose-*g*-polyacrylamide/montmorillonite for colon targeted drug deliver. Nanomed Res J. 2017;2:111–22. doi: 10.22034/NMRJ.2017.58964.1058.
[30] Goncharuk O, Samchenko Y, Sternik D, Kernosenko L, Poltorats'ka T, Partmurska N, et al. Thermosensitive hydrogel nanocomposites with magnetic laponite nanoparticles. Appl Nanosci. 2020. doi: 10.1007/s13204-020-01388-w.
[31] Fayazi M. Chemistry facile hydrothermal synthesis of magnetic sepiolite clay for removal of Pb(II). Anal Bioanal Chem Res. 2019;6(1):125–36. doi: 10.22036/ABCR.2018.141470.1227.
[32] Magdy A, Fouad YO, Abdel-Aziz MH, Konsowa AH. Synthesis and characterization of Fe_3O_4/kaolin magnetic nanocomposite and its application in wastewater treatment. J Ind Eng Chem. 2017;56:299–311. doi: 10.1016/j.jiec.2017.07.023.
[33] Tokarčíková M, Tokarský J, Kutláková KM, Seidlerová J. Testing the stability of magnetic iron oxides/kaolinite nanocomposite under various pH conditions. J Solid State Chem. 2017;253:329–35. doi: 10.1016/j.jssc.2017.06.004.
[34] Zong P, Wang S, He C. Synthesis of kaolinite/iron oxide magnetic composites and their use in the removal of Cd(II) from aqueous solutions. Water Sci Technol. 2013;67:1642–9. doi: 10.2166/wst.2013.012.
[35] Xie Y, Qian D, Wu D, Ma X. Magnetic halloysite nanotubes/iron oxide composites for the adsorption of dyes. Chem Eng J. 2011;168:959–63. doi: 10.1016/j.cej.2011.02.031.
[36] Tsoufis T, Katsaros F, Kooi BJ, Bletsa E, Papageorgiou S, Deligiannakis Y, et al. Halloysite nanotube-magnetic iron oxide nanoparticle hybrids for the rapid catalytic decomposition of pentachlorophenol. Chem Eng J. 2017;313:466–74. doi: 10.1016/j.cej.2016.12.056.
[37] Rahmani S, Zeynizadeh B, Karami S. Removal of cationic methylene blue dye using magnetic and anionic-cationic modified montmorillonite: kinetic, isotherm and thermodynamic studies. Appl Clay Sci. 2020;184:105391. doi: 10.1016/j.clay.2019.105391.
[38] Cho DW, Jeon BH, Chon CM, Kim Y, Schwartz FW, Lee ES, et al. A novel chitosan/clay/magnetite composite for adsorption of Cu(II) and As(V). Chem Eng J. 2012;200–202:654–62. doi: 10.1016/j.cej.2012.06.126.
[39] Tireli AA, do Rosário Guimarães I, de Souza Terra JC, da Silva RR, Guerreiro MC. Fenton-like processes and adsorption using iron oxide-pillared clay with magnetic properties for organic compound mitigation. Environ Sci Pollut Res. 2014;22:870–81. doi: 10.1007/s11356-014-2973-x.

[40] Mao H, Liu X, Yang J, Li B, Yao C, Kong Y. Synthesis of magnetic FexOy@silica-pillared clay (SPC) composites via a novel sol-gel route for controlled drug release and targeting. Mater Sci Eng C. 2014;40:102–8. doi: 10.1016/j.msec.2014.03.040.

[41] Rezvani Z, Sarkarat M. Synthesis and characterization of magnetic composites: intercalation of naproxen into Mg–Al layered double hydroxides coated on Fe_3O_4. Z Anorg Allg Chem. 2012;638:874–80. doi: 10.1002/zaac.201100487.

[42] Miranda LD, Bellato CR, Milagres JL, Moura LG, Mounteer AH, de Almeida MF. Hydrotalcite-TiO_2 magnetic iron oxide intercalated with the anionic surfactant dodecylsulfate in the photocatalytic degradation of methylene blue dye. J Env Manage. 2015;156:225–35. doi: 10.1016/j.jenvman.2015.03.051.

[43] Miranda LD, Bellato CR, Fontes MP, Moura LG, Mounteer AH, de Almeida MF. Preparation and evaluation of hydrotalcite-iron oxide magnetic organocomposite intercalated with surfactants for cationic methylene blue dye removal. Chem Eng J. 2014;254:88–97. doi: 10.1016/j.cej.2014.05.094.

[44] Lu L, Li J, Ng DH, Yang P, Song P, Zuo M. Synthesis of novel hierarchically porous Fe_3O_4@MgAl–LDH magnetic microspheres and its superb adsorption properties of dye from water. J Ind Eng Chem. 2017;46:315–23. doi: 10.1016/j.jiec.2016.10.045.

[45] Zhao S, Wu M, Jing R, Liu X, Shao Y, Zhang Q, et al. One-pot formation of magnetic layered double hydroxide based on electrostatic self-assembly to remove Cr(VI) from wastewater. Appl Clay Sci. 2019;182:105297. doi: 10.1016/j.clay.2019.105297.

[46] Wu D, Zhu C, Chen Y, Zhu B, Yang Y, Wang Q, et al. Preparation, characterization and adsorptive study of rare earth ions using magnetic GMZ bentonite. Appl Clay Sci. 2012;62–63:87–93. doi: 10.1016/j.clay.2012.04.015.

[47] Zhang B, Zhang T, Zhang Z, Xie M. Hydrothermal synthesis of a graphene/magnetite/montmorillonite nanocomposite and its ultrasonically assisted methylene blue adsorption. J Mater Sci. 2019;54:11037–55. doi: 10.1007/s10853-019-03659-6.

[48] Zou C, Liang J, Jiang W, Guan Y, Zhang Y. Adsorption behavior of magnetic bentonite for removing Hg(II) from aqueous solutions. RSC Adv. 2018;8:27587–95. doi: 10.1039/c8ra05247f.

[49] Peng G, Li T, Ai B, Yang S, Fu J, He Q, et al. Highly efficient removal of enrofloxacin by magnetic montmorillonite via adsorption and persulfate oxidation. Chem Eng J. 2019;360:1119–27. doi: 10.1016/j.cej.2018.10.190.

[50] Ouali A, Belaroui LS, Bengueddach A, Galindo AL, Peña A. Fe_2O_3-palygorskite nanoparticles, efficient adsorbates for pesticide removal. Appl Clay Sci. 2015;115:67–75. doi: 10.1016/j.clay.2015.07.026.

[51] Xu X, Chen W, Zong S, Ren X, Liu D. Magnetic clay as catalyst applied to organics degradation in a combined adsorption and fenton-like process. Chem Eng J. 2019;373:140–9. doi: 10.1016/j.cej.2019.05.030.

[52] Chen Y, Zhu B, Wu D, Wang Q, Yang Y, Ye W, et al. Eu(III) adsorption using di(2-thylhexly) phosphoric acid-immobilized magnetic GMZ bentonite. Chem Eng J. 2012;181–182:387–96. doi: 10.1016/j.cej.2011.11.100

[53] Liu K, Tong Z, Muhammad Y, Huang G, Zhang H, Wang Z, et al. Synthesis of sodium dodecyl sulfate modified BiOBr/magnetic bentonite photocatalyst with Three-dimensional parterre like structure for the enhanced photodegradation of tetracycline and ciprofloxacin. Chem Eng J. 2020;388:124374. doi: 10.1016/j.cej.2020.124374.

[54] Wu D, Zheng P, Chang PR, Ma X. Preparation and characterization of magnetic rectorite/iron oxide nanocomposites and its application for the removal of the dyes. Chem Eng J. 2011;174:489–94. doi: 10.1016/j.cej.2011.09.029.

[55] Liu H, Chen W, Liu C, Liu Y, Dong C. Magnetic mesoporous clay adsorbent: preparation, characterization and adsorption capacity for atrazine. Microporous Mesoporous Mater. 2014;194:72–8. doi: 10.1016/j.micromeso.2014.03.038

[56] Zhang R. Investigation of magnetic modified clay nano-adsorbents in removing micro-pollution from potable water. In: International Conference on Biological, Chemical & Environmental Sciences (BCES-2016). 2016; p. 6–11. doi: 10.15242/iicbe.c0816201.

[57] Shah KH, Ali S, Shah F, Waseem M, Ismail B, Khan RA, et al. Magnetic oxide nanoparticles (Fe_3O_4) impregnated bentonite clay as a potential adsorbent for Cr(III) adsorption. Mater Res Express. 2018;5:1. doi: 10.1080/17425247.2018.1544616.

[58] Makarchuk OV, Dontsova TA, Astrelin IM. Magnetic clay sorbent for the removal of dyes from aquoeus solutions. ХІМІЧНІ ТЕХНОЛОГІЇ. 2016;5:109–14.

[59] Zhang H, Omer AM, Hu Z, Yang LY, Ji C, Ouyang XK. Fabrication of magnetic bentonite/carboxymethyl chitosan/sodium alginate hydrogel beads for Cu(II)adsorption. Int J Biol Macromol. 2019;135:490–500. doi: 10.1016/j.ijbiomac.2019.05.185

[60] Hashemian S. $MnFe_2O_4$/bentonite nano composite as a novel magnetic material for adsorption of acid red 138. Afr J Biotechnol. 2010;9:8667–71. doi: 10.5897/AJB09.1296

[61] Lasheen MR, El-Sherif IY, Sabry DY, El-Wakeel ST, El-Shahat MF. Adsorption of heavy metals from aqueous solution by magnetite nanoparticles and magnetite–kaolinite nanocomposite: equilibrium, isotherm and kinetic study. Desalin Water Treat. 2016;57:17421–9. doi: 10.1080/19443994.2015.1085446.

[62] Wang Z, Yang X, Qin T, Liang G, Li Y, Xie X. Efficient removal of oxytetracycline from aqueous solution by a novel magnetic clay–biochar composite using natural attapulgite and cauliflower leaves. Environ Sci Pollut Res. 2019;26:7463–75. doi: 10.1007/s11356-019-04172-8.

[63] Balbino TA, Bellato CR, da Silva AD, Neto JD, Ferreira SO. Preparation and evaluation of iron oxide/hydrotalcite intercalated with dodecylsulfate/β-cyclodextrin magnetic organocomposite for phenolic compounds removal. Appl Clay Sci. 2020;193:105659. doi: 10.1016/j.clay.2020.105659.

[64] Janacek D, Kvitek L, Karlikova M, Pospiskova K, Safarik I. Removal of silver nanoparticles with native and magnetically modified halloysite. Appl Clay Sci. 2018;162:10–4. doi: 10.1016/j.clay.2018.05.024.

[65] Riahi-Madvaar R, Taher MA, Fazelirad H. Synthesis and characterization of magnetic halloysite-iron oxide nanocomposite and its application for naphthol green B removal. Appl Clay Sci. 2017;137:101–6. doi: 10.1016/j.clay.2016.12.019.

[66] Fayazi M, Afzali D, Taher MA, Pospiskova K, Safarik I. Removal of safranin dye from aqueous solution using magnetic mesoporous clay: optimization study. J Mol Liq. 2015;212:675–85. doi: 10.1016/j.molliq.2015.09.045.

[67] Fayazi M, Afzali D, Taher MA, Mostafavi A, Gupta VK. A magnetic core-shell dodecyl sulfate intercalated layered double hydroxide nanocomposite for the adsorption of cationic and anionic organic dyes. Appl Clay Sci. 2019;183:105309. doi: 10.1016/j.clay.2019.105309.

[68] Peng X, Luan Z, Zhang H. Montmorillonite-Cu(II)/Fe(III) oxides magnetic material as adsorbent for removal of humic acid and its thermal regeneration. Chemosphere. 2006;63:300–6. doi: 10.1016/j.chemosphere.2005.07.019.

[69] Mu B, Tang J, Zhang L, Wang A. Preparation, characterization and application on dye adsorption of a well-defined two-dimensional superparamagnetic clay/polyaniline/Fe_3O_4 nanocomposite. Appl Clay Sci. 2016;132–133:7–16. doi: 10.1016/j.clay.2016.06.005.

[70] Yu J, Yang Q-X. Magnetization improvement of Fe-pillared clay with application of polyetheramine. Appl Clay Sci. 2010;48:185–90. doi: 10.1016/j.clay.2009.12.007.

[71] Chen L, Huang Y, Huang L, Liu B, Wang G, Yu S. Characterization of Co(II) removal from aqueous solution using bentonite/iron oxide magnetic composites. J Radioanal Nucl Chem. 2011;290:675–84. doi: 10.1007/s10967-011-1337-y.

[72] Marco-Brown JL, Barbosa-Lema CM, Sánchez RM, Mercader RC, dos Santos Afonso M. Adsorption of picloram herbicide on iron oxide pillared montmorillonite. Appl Clay Sci. 2012;58:25–33. doi: 10.1016/j.clay.2012.01.004.

[73] Ouachtak H, El Haouti R, El Guerdaoui A, Haounati R, Amaterz E, Addi AA, et al. Experimental and molecular dynamics simulation study on the adsorption of Rhodamine B dye on magnetic montmorillonite composite γ-Fe_2O_3@Mt. J Mol Liq. 2020;309:113142. doi: 10.1016/j.molliq.2020.113142.

[74] Galeano LA, Bravo PF, Luna CD, Vicente MÁ, Gil A. Removal of natural organic matter for drinking water production by Al/Fe-PILC-catalyzed wet peroxide oxidation: effect of the catalyst preparation from concentrated precursors. Appl Catal B Env. 2012;111–112:527–35. doi: 10.1016/j.apcatb.2011.11.004.

[75] Zong S, Xu X, Ran G, Liu J. Comparative study of atrazine degradation by magnetic clay activated persulfate and H_2O_2. RSC Adv. 2020;10:11410–7. doi: 10.1039/d0ra00345j.

[76] Bao T, Damtie MM, Wu K, Wei XL, Zhang Y, Chen J, et al. Rectorite-supported nano-Fe_3O_4 composite materials as catalyst for *P*-chlorophenol degradation: preparation, characterization, and mechanism. Appl Clay Sci. 2019;176:66–77. doi: 10.1016/j.clay.2019.04.020.

[77] Yang S, Wu P, Liu J, Chen M, Ahmed Z, Zhu N. Efficient removal of bisphenol a by superoxide radical and singlet oxygen generated from peroxymonosulfate activated with Fe0-montmorillonite. Chem Eng J. 2018;350:484–95. doi: 10.1016/j.cej.2018.04.175.

[78] Song XC, Qi YL, Zheng YF, Liu JN, Yin HY. Construction of magnetic Fe_3O_4@C@Ag_3PO_4 nanocomposites with excellent visible photocatalytic performance. J Nanosci Nanotechnol. 2017;17:1407–12. doi: 10.1166/jnn.2017.12723.

[79] Son YH, Lee JK, Soong Y, Martello D, Chyu MK. Heterostructured zero valent iron-montmorillonite nanohybrid and their catalytic efficacy. Appl Clay Sci. 2012;62–63:21–6. doi: 10.1016/j.clay.2012.04.003.

[80] Lian J, Ouyang Q, Tsang PE, Fang Z. Fenton-like catalytic degradation of tetracycline by magnetic palygorskite nanoparticles prepared from steel pickling waste liquor. Appl Clay Sci. 2019;182:105273. doi: 10.1016/j.clay.2019.105273.

[81] Hou K, Wang G, Zhu Y, Ezzatahmadi N, Fu L, Tang A, et al. Sepiolite/Fe_3O_4 composite for effective degradation of diuron. Appl Clay Sci. 2019;181:105243. doi: 10.1016/j.clay.2019.105243.

[82] Rouhi M, Babamoradi M, Hajizadeh Z, Maleki A, Maleki ST. Design and performance of polypyrrole/halloysite nanotubes/Fe_3O_4/Ag/Co nanocomposite for photocatalytic degradation of methylene blue under visible light irradiation. Opt (Stuttg). 2020;212:164721. doi: 10.1016/j.ijleo.2020.164721.

[83] Wang J, Chen Y, Liu G, Cao Y. Synthesis, characterization and photocatalytic activity of inexpensive and non-toxic Fe_2O_3–Fe_3O_4 nano-composites supported by montmorillonite and modified by graphene. Compos Part B Eng. 2017;114:211–22. doi: 10.1016/j.compositesb.2017.01.055.

[84] Jin M, Long M, Su H, Pan Y, Zhang Q, Wang J, et al. Magnetically separable maghemite/montmorillonite composite as an efficient heterogeneous fenton-like catalyst for phenol degradation. Environ Sci Pollut Res. 2017;24:1926–37. doi: 10.1007/s11356-016-7866-8.

[85] Bledowski M, Wang L, Ramakrishnan A, Khavryuchenko OV, Khavryuchenko VD, Ricci PC, et al. Visible-light photocurrent response of TiO_2-polyheptazine hybrids: evidence for interfacial charge-transfer absorption. Phys Chem Chem Phys. 2011;13:21511–9. doi: 10.1039/c1cp22861g.

[86] Dong H, Zhang X, Li J, Zhou P, Yu S, Song N, et al. Construction of morphology-controlled nonmetal 2D/3D homojunction towards enhancing photocatalytic activity and mechanism insight. Appl Catal B. 2020;263:118270. doi: 10.1016/j.apcatb.2019.118270.

[87] Siregar SH, Wijaya K, Kunarti ES, Syoufian A. Synthesis and characteristics of the magnetic properties of Fe_3O_4-(CTAB-montmorillonite) composites, based on variation in Fe^{3+}/Fe^{2+} concentrations. Orient J Chem. 2018;34:716–22. doi: 10.13005/ojc/340213.

[88] Nogueira FG, Lopes JH, Silva AC, Lago RM, Fabris JD, Oliveira LC. Catalysts based on clay and iron oxide for oxidation of toluene. Appl Clay Sci. 2011;51:385–9. doi: 10.1016/j.clay.2010.12.007.